Comparative analysis of optoacoustic pulses in aluminum and silicon

O. N. Koroleva[a)]

Moscow Humanitarian University, Moscow

A. V. Mazhukin[b)]

M. V. Keldysh Institute of Applied Mathematics, Russian Academy of Sciences, Moscow

(Submitted February 18, 2011)
Opticheskiĭ Zhurnal **78**, 79–89 (August 2011)

The methods of mathematical modeling are used for a comparative analysis of the optoacoustic response to a short moderate-intensity laser pulse acting on aluminum and silicon. Regimes of action close to the experimental data are considered, in which laser pulses of identical width 3×10^{-9} s were used, with their intensity varying within the limits 10^7–10^{10} W/cm^2.

INTRODUCTION

The explosive development of laser technologies in various areas of the processing and creation of new materials has attracted attention in recent decades to research into the processes that occur in the zone of laser action and to a basic means of such research—optoacoustic diagnosis.[1–4] Optoacoustic diagnosis is an accurate and sensitive method of comprehensively describing the dynamics of processes as they occur. The greatest interest for laser technologies is presented by pulsed laser action of moderate intensity ($G \leq 10^{10}$ W/cm^2). The action of laser radiation on absorbing condensed media is accompanied by the generation of pressure pulses that carry information on the character of the processes in the irradiation zone. Optoacoustics is based on measuring the acoustic fields excited by laser action in condensed media. The measurement of acoustic signals in terms of a one-dimensional spatial model reduces to recording the time scan of a pressure pulse $P(t)$. Because the experimental implementation is relatively simple, acoustic methods cover a wide range of intensity 10^6–10^{10} W/cm^2 and time of action 10^{-9}–10^{-3} s. In a number of applied problems, acoustic methods make it possible to obtain information on processes in condensed media that cannot be achieved for other measurement methods. It has turned out that studying the shape of acoustic signals is an effective way to study the dynamics of rapid phase transitions when nano- and microsecond laser pulses are acting on condensed media.[5]

In interpreting signals obtained experimentally, it is hard to establish by what combination of processes they were formed if there is no qualitative information on the behavior and relative contribution to the signal of various processes. Modern methods of mathematical modelling provide a tool for obtaining such information.

This paper is devoted to a study of the features of the optoacoustic signals that arise in connection with the melting and vaporization of the substance in the zone of laser irradiation of aluminum and silicon.

FORMULATION OF THE PROBLEM

A laser pulse of nanosecond width with intensity 10^7–10^9 W/cm^2 acts on the free surface of a flat, strongly absorbing plate. The energy of the pulse is absorbed in a thin near-surface zone of the target, and this causes it to be heated, melted, and vaporized. Under the action of thermal expansion and phase transformations, a pressure signal (an optoacoustic signal), which propagates toward the opposite fixed side is formed close to the surface. The radius r of the focusing spot of the laser radiation is assumed to be much greater than the penetration depth of the laser radiation, $r \gg (\chi \tau_L)^{1/2}$, where χ is the thermal conductivity ($\chi = 1.01$ cm^2/s for silicon, and $\chi = 0.99$ cm$^2/s$ for aluminum), and τ_L is the half-width of the laser pulse. The intensity distribution in the plane of the spot is assumed to be uniform, and this makes it possible to use a spatially one-dimensional approximation to mathematically describe it, Fig. 1.

The processes of formation and propagation of an optoacoustic signal were mathematically modelled in terms of a combined version of the hydrodynamic Stefan problem[6] that includes the classical and single-phase version. The basis of the combined version is a system of equations of hydrodynamics, supplemented by the equation of laser-radiation transport in the material. The hydrodynamic system includes equations of continuity, motion, and total energy. Convective, conductive, and radiative transport mechanisms are taken into account. In divergent form, the system of equations has the form

$$\left[\frac{\partial \rho}{\partial t} + \frac{\partial}{\partial x}(\rho u) = 0\right]_k, \tag{1}$$

$$\left[\frac{\partial}{\partial t}(\rho u) + \frac{\partial}{\partial x}(\rho u^2) = -\frac{\partial p}{\partial x}\right]_k, \tag{2}$$

$$\left[\frac{\partial}{\partial t}\left(\rho\left(H + \frac{u^2}{2}\right)\right) + \frac{\partial}{\partial x}\left(\rho u\left(H + \frac{u^2}{2}\right)\right) = -\frac{\partial}{\partial x}(pu) - \frac{\partial W}{\partial x} - \frac{\partial G}{\partial x}\right]_k, \tag{3}$$

 1070-9762/2011/080529-08/$15.00

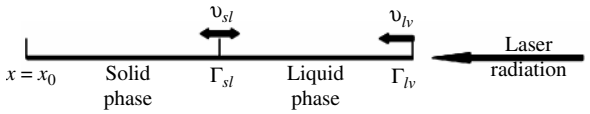

FIG. 1. Spatial location of the phases and interphase boundaries when a laser acts on a target: Γ_{lv} is the vaporization boundary, Γ_{sl} is the solid–liquid interface, v_{lv} and v_{sl} are the speeds of the vaporization and melting boundaries.

$$\left[\frac{\partial G}{\partial x} + \alpha G = 0\right]_k \quad x \in [x_0, \Gamma_{sl}] \cup [\Gamma_{sl}, \Gamma_{lv}]$$
$$k = \begin{cases} s, x \in [x_0, \Gamma_{sl}] \\ l, x \in [\Gamma_{s\ell}, \Gamma_{lv}]. \end{cases} \tag{4}$$

The following relationships were used as the equations of state:

$$H_l = c_{pl}T_l \quad p_l = u_c^2\rho_{0l}\left(\left(\frac{\rho}{\rho_{0l}} - 1\right) + \beta_l(T - T_m)\right)$$
$$x \in [\Gamma_{lv}, \Gamma_{sl}]. \tag{5}$$
$$H_s = c_{ps}T_s \quad p_s = u_c^2\rho_{0s}\left(\left(\frac{\rho}{\rho_{0s}} - 1\right) + \beta_s(T - T_0)\right)$$
$$x \in [\Gamma_{sl}, x_s]. \tag{6}$$

The following notation and units are used in the system of equations under consideration: ρ[g/cm^3] is the density, u [cm/s] and p [bar] are the hydrodynamic velocity and pressure, u_c [cm/s] is the speed of sound, H[J/cm^3] is the enthalpy, W [W/cm^2] is the heat flow, α [1/cm] is the absorption coefficient of the laser radiation, G[W/cm^2] is the power density of the laser radiation, c_p [J/g K] is the heat capacity at constant pressure, β [1/K] is the thermal coefficient of linear expansion, T_0 [K] is room temperature, T_m [K] is the equilibrium melting temperature, and $\rho_{0,s}$ and $\rho_{0,l}$ are the initial densities of the solid and liquid phases, specified, respectively, at temperatures T_0 and T_m. Subscripts *sur*, *s*, *l*, and *v* indicate that the quantities relate to the surface and to solid, liquid, and vapor media, respectively, while subscripts *sl* and *lv* denote membership in interphase solid–liquid interfaces, $x = \Gamma_{sl}$ and the vaporization boundary Γ_{lv}. The system of Eqs. (1)–(6) was supplemented with boundary conditions and initial conditions:

The left boundary $x = x_0$, assuming it to be fixed and thermally insulated (Fig. 1).

$$x = x_0 : \lambda\frac{\partial T_s}{\partial x} = 0, \qquad u_s = 0. \tag{7}$$

A model of the surface melting, consisting of three laws of conservation, supplemented with the continuity condition for the temperature of the phase transition, is formed at the interphase boundary $x = \Gamma_{sl}$.

$$x = \Gamma_{sl} : \rho_s\upsilon_{sl} = \rho_l(u_s - u_l + \upsilon_{sl}), \tag{8}$$
$$\rho_s\upsilon_{sl}^2 + p_s = \rho_l(u_s - u_l + \upsilon_{sl})^2 + p_l, \tag{9}$$
$$\lambda_l\frac{\partial T_l}{\partial x} - \lambda_s\frac{\partial T_s}{\partial x} = L_m^{ne}\rho_s\upsilon_{sl}, \tag{10}$$
$$T_s = T_l = T_{sl} = T_m, \tag{11}$$

where

$$L_m^{ne} = L_m + (c_{pl} - c_{ps})(T_{sl} - T_{m,0}) + \frac{\rho_s + \rho_l}{\rho_s - \rho_l}\frac{(u_s - u_l)^2}{2}$$

is the nonequilibrium heat of melting, L_m [J/g] is the equilibrium heat of melting, and λ [W/cm K] is the thermal conductivity.

A model of the surface vaporization is formed at the right of the irradiated boundary $x = \Gamma_{lv}(t)$, written in the approximation of the Knudsen layer and consisting of three laws of conservation and two supplementary conditions that characterize the degree of nonequilibrium of the phase transition:

$$x = \Gamma_{l\upsilon} : \rho_l\upsilon_{l\upsilon} = \rho_\upsilon(\upsilon_{l\upsilon} + u_l - u_\upsilon), \tag{12}$$
$$p_l + \rho_l\upsilon_{l\upsilon}^2 = p_\upsilon + \rho_\upsilon(\upsilon_{l\upsilon} + u_l - u_\upsilon)^2, \tag{13}$$
$$W_l^T = \lambda_l\frac{\partial T_l}{\partial x} = \rho_l\upsilon_{l\upsilon}L_\upsilon^{ne} + \sigma T_{sur}^4, \tag{14}$$
$$T_\upsilon = T_l\alpha_T(M), \qquad \rho_\upsilon = \rho_{sat}\alpha_\rho(M), \tag{15}$$
$$G_{l\upsilon} = A(T_{sur})G_\upsilon \exp\left(-4\left(\frac{t}{\tau_L}\right)^2\right), \tag{16}$$

where

$$L_\upsilon^{ne} = L_\upsilon(T_l) + c_{p\upsilon}(T_l - T_\upsilon) + \frac{\rho_l + \rho_\upsilon}{\rho_l - \rho_\upsilon}\frac{(u_l - u_\upsilon)^2}{2}$$

is the nonequilibrium heat of vaporization, G_{lv} and G_0 are the laser-radiation energy absorbed by the surface and its maximum value, A_{sur}[%] is the surface absorptivity, τ_L [ns] is the half-width of the laser pulse, L_v [J/g] is the heat of vaporization, $M = u_{lv}/u_s$ is the Mach number, $u_s = (\gamma RT_v)^{1/2}$ is the speed of sound on the outside of the Knudsen layer, $\gamma = c_p/c_v$, R [J/g K] is the universal gas constant, and $\alpha_T(M)$ and $\alpha_\rho(M)$ are the Crout coefficients.[7,8] When $M = 1$, $\alpha_T(M) = 0.633$ and $\alpha_\rho(M) = 0.326$.

The saturated vapor pressure was computed, using the Clausius–Clapeyron equations:

$$p_{sat} = p_b \exp\left(\frac{L_\upsilon\mu}{RT_b}\left(1 - \frac{T_b}{T_l}\right)\right), \qquad \rho_{sat} = p_{sat}/RT_l, \tag{17}$$

where p_b and T_b are, respectively, the pressure and temperature of boiling under normal conditions. At the initial instant t_0, the temperature and density are assumed constant, while the velocity is zero:

$$T_s = T_0, \qquad \rho_s = \rho_{0,s}, \qquad u_s = 0. \tag{18}$$

OPTICAL AND THERMOPHYSICAL CHARACTERISTICS OF ALUMINUM AND SILICON

The thermophysical and optical characteristics of the target material have a strong effect on the shape of the optoacoustic signals.[9,10] The characteristics of the materials used in the calculations, presented in Figs. 2(a), 2(b), and 3, are taken from handbook data.[11,12] The vertical lines on the figures indicate the equilibrium melting and vaporization

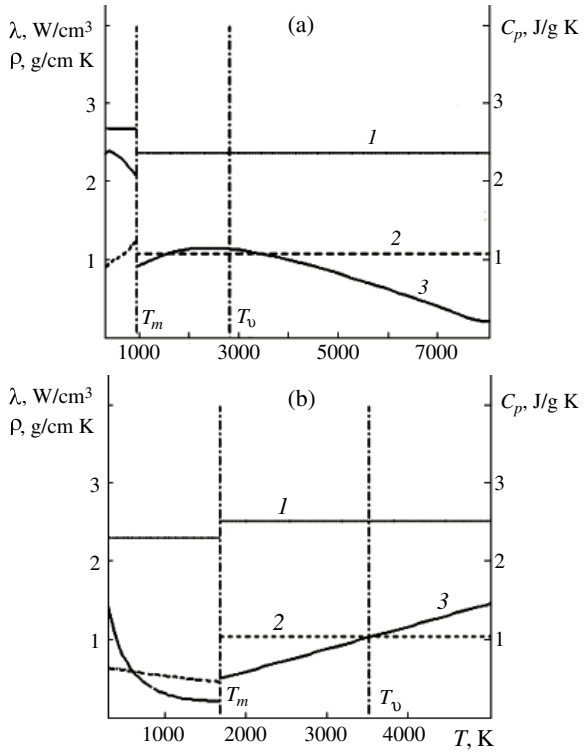

FIG. 2. Thermophysical characteristics of aluminum (a) and silicon (b). *1*—Density, *2*—heat capacity, *3*—thermal conductivity; T_m is the melting temperature, and T_v is the vaporization temperature.

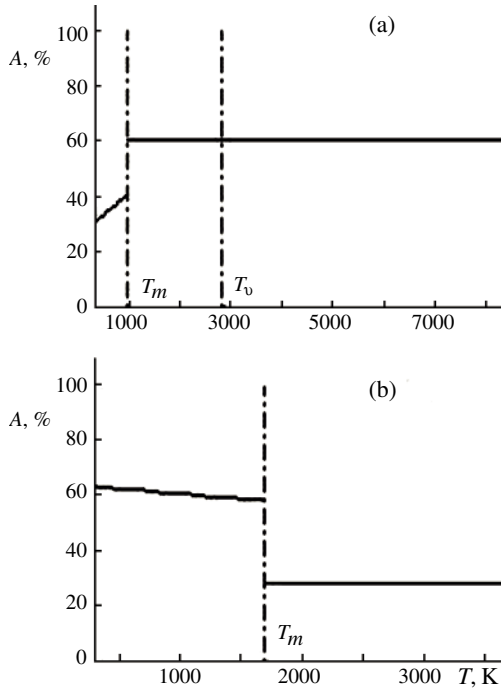

FIG. 3. Absorptivity of aluminum (a) and silicon (b). *1*—Density, *2*—heat capacity, *3*—thermal conductivity; T_m is the melting temperature, and T_v is the vaporization temperature.

temperatures of each of the materials. All the thermophysical and optical characteristics of both materials break down as they pass through the equilibrium melting temperature (shown in Figs. 2 and 3 by vertical lines). Recalling that one of the materials under consideration is a metal, while the other is a semiconductor, their thermophysical and optical characteristics are very different. As the melting front is passed through, the thermophysical characteristics of aluminum decrease abruptly, while those of silicon increase. Table 1 shows the values of the thermophysical parameters that characterize the properties of the materials under consideration.

Solution algorithm. In terms of computation, the main complication in solving the Stefan problem consists of the presence of several (in our case, two) moving boundaries whose positions are unknown and must be determined in the course of the calculations, with the sizes of the solid and liquid subregions being able to change by several orders of magnitude in the process of the calculations. The analysis of what the phase transition contributes to the optoacoustic signal requires the position of the interphase boundary and its speed to be accurately determined. The most efficient way to solve this problem is by the method of dynamic adaptation,[13–16] which makes it possible to carry out the calculation with the interphase boundaries clearly distinguished.

The method of dynamic adaptation. The numerical solution of the problem of Eqs. (1)–(18) is carried out by the method of dynamic adaptation, which is based on the idea of converting to an arbitrary nonsteady-state coordinate system, which can be accomplished with the help of the desired solution. In an arbitrary nonsteady-state coordinate system, the problem is described by an expanded differential system of equations, part of which describe the physical phenomena, while another part describes the dynamics of the nodes of the calculational network. The problems associated with movable boundary conditions are eliminated by going to an arbitrary nonsteady-state coordinate system in which the network nodes and the boundaries are nonmoving. The coordinates are automatically transformed by means of the desired solution, and this makes it possible to arrange the network nodes as a function of the features of the solution.

The transition from physical space with variables (x, t) to a calculated space with an arbitrary nonsteady-state coordinate system (q, τ) is accomplished by replacing them with variables of the general form

$$x = f(q, \tau), \qquad t = \tau, \tag{19}$$

having the inverse nondegenerate transformation

$$q = \varphi(x, t), \qquad \tau = t.$$

The partial derivatives in the (q, τ) coordinate system have the form

$$\frac{\partial}{\partial x} = \frac{1}{\psi}\frac{\partial}{\partial q}, \qquad \frac{\partial}{\partial t} = \frac{\partial}{\partial \tau} + \frac{Q}{\psi}\frac{\partial}{\partial q}, \tag{20}$$

where $\partial x/\partial \delta = -Q$ is the velocity of the new coordinate system relative to the original one, which is to be determined below.

In the nonsteady-state coordinate system, two phase subregions $[\Gamma_{lv}, \Gamma_{sl}] \cup [\Gamma_{sl}, x_s]$ with movable boundaries Γ_{lv} and Γ_{sl} are mapped into two calculated subregions $[0, q_{sl}]$ and $[q_{sl}, q_s]$ with fixed boundaries. Until the liquid phase appears,

TABLE 1. Thermophysical parameters of aluminum and silicon

Mineral	Atomic weight, g/mol	Temperature T_m, K	T_b, K	Thermal expansion coefficient, 1/K Solid phase β_s	Liquid β_l	Heat of transition Melting L_m (J/g)	Boiling L_b (J/g)
Al	26.98	933	2793	2.33×10^{-5}	5.00×10^{-5}	400.30	10,860
Si	28	1683	3514	4.65×10^{-3}	1.40×10^{-4}	1797.0	13,720

the physical region $[\Gamma_{lv}, x_s]$ is mapped onto the calculated subregion $[0, q_s]$. Physical coordinate x in the calculated space becomes the new unknown function. In the new coordinate system, the dynamics of the calculational network is described by a supplementary differential equation:

$$\left[\frac{\partial \psi}{\partial \tau} = -\frac{\partial Q}{\partial q}\right]_k \quad k = s, l, \tag{21}$$

where $\psi = \partial x/\partial q$ is the metric coefficient, Q is a function that determines the specific form of the transformation in accordance with the features of the problem.

Using the transformation of variables given by Eqs. (19), we write the differential problem given by Eqs. (1)–(17) in an arbitrary nonsteady-state coordinate system (q, τ):

$$\begin{aligned}
&\left[\frac{\partial(\psi\rho)}{\partial\tau} + \frac{\partial}{\partial q}(\rho(u+Q)) = 0\right]_k,\\
&\left[\frac{\partial}{\partial\tau}(\psi\rho u) + \frac{\partial}{\partial q}(\rho u(u+Q)) = -\frac{\partial p}{\partial q}\right]_k,\\
&\left[\frac{\partial}{\partial\tau}\left(\psi\rho\left(H+\frac{u^2}{2}\right)\right) + \frac{\partial}{\partial q}\left(\rho(u+Q)\left(H+\frac{u^2}{2}\right)\right)\right.\\
&\quad \left. = -\frac{\partial}{\partial q}(pu) + \frac{\partial}{\partial q}\left(\frac{\lambda(T)}{\psi}\frac{\partial T}{\partial q}\right)\right]_k,\\
&\left[\frac{\partial G}{\partial q} + \alpha\psi G = 0\right]_k,\\
&q \in [0, q_{sl}] \cup [q_{sl}, q_s], \qquad \tau \in [\tau_0, \tau_{end}], \qquad k = s, l.
\end{aligned} \tag{22}$$

The boundary conditions are

$$q = q_0 : u = W = 0, \qquad Q = 0; \tag{23}$$

$$q = \Gamma_{sl} : \rho_s(Q_{sl} + u_s) = \rho_l(Q_{sl} + u_l), \tag{24}$$

$$p_s + \rho_s(Q_{sl} + u_s)^2 = p_l + \rho_l(Q_{sl} + u_l)^2, \tag{25}$$

$$W_l - W_s = \rho_s \upsilon_{sl} L_m^{ne}, \quad \upsilon_{sl} = Q_{sl} + u_s. \tag{26}$$

$$q = \Gamma_{l\upsilon} : \rho_l(Q_{l\upsilon} + u_l) = \rho_\upsilon(Q_{l\upsilon} + u_\upsilon), \tag{27}$$

$$p_l + \rho_l(Q_{l\upsilon} + u_l)^2 = p_\upsilon + \rho_\upsilon(Q_{l\upsilon} + u_\upsilon)^2, \tag{28}$$

$$\begin{aligned}
&W_l^T = W_l^T - \frac{\lambda_l}{\psi_l}\frac{\partial T_l}{\partial q} = \rho_l \upsilon_{l\upsilon} L_\upsilon^{ne} + \sigma T_{sur}^4,\\
&\upsilon_{l\upsilon} = -(Q_{l\upsilon} + u_l),\\
&G_{l\upsilon} = A(T_{sur}) G_0 \exp\left(-4\left(\frac{\tau}{\tau_L}\right)^2\right).
\end{aligned} \tag{29}$$

$$\tau = \tau_0 : T_s = T_0, \qquad u_s = 0, \qquad \rho_s = \rho_{0,s}, \qquad \psi = 1. \tag{30}$$

Thus, by going to an arbitrary nonsteady-state coordinate system, the original differential model is transformed into the expanded differential system of Eqs. (21)–(30), in which a supplementary equation of the type of Eq. (21) appears, being the equation of the inverse transformation. Its type, properties, and the form of its boundary conditions depend on the specific form of function Q. To construct uniform (quasi-uniform) networks at each instant in regions with moving boundaries, function Q is given in the form[13,14]

$$\left[Q = -D\frac{\partial \psi}{\partial q}\right]_k, \quad k = s, l,$$

where diffusion coefficient D is expressed in terms of the geometrical and speed parameters of the problem: $D = L^2(t)(|v_{sl}| + |v_{lv}|)/\Delta x$.

The difference approximation. The differential model of Eqs. (21)–(30) is solved numerically by using the finite difference method, according to which the equations of hydrodynamics were approximated by a family of conservative difference schemes obtained by the integro-interpolation method.[17] To construct the family of difference schemes, the network ω_q^τ with nonuniform steps $h_{k,i}$ and τ^j is introduced in the calculational space with spatial variable q and temporal variable τ: $\omega = \{\omega_l \cup \omega_s\} \times \{\omega_\tau\}$(see Box 1 for definitions of ω_l, ω_s, and ω_τ).

In the difference approximation of the equations, the nodes with integral subscripts relate to network functions p, Q, x, and the points with half-integral subscripts $(q_{m+1/2}, \tau^j)$ relate to network functions ψ, ρ, u, T. The system of Eqs. (22) was approximated by means of a completely implicit difference scheme having an approximation order of $Q(\tau + h)$.

For the differential system of Eqs. (21) and (22), the family of difference schemes has the form

$$\left\{\frac{(\psi\rho)_{i+1/2}^{j+1} - (\psi\rho)_{i+1/2}^{j}}{\Delta\tau^{j+1}} + \frac{[\rho(u+Q)]_{i+1}^{j+1} - [\rho(u+Q)]_i^{j+1}}{h_{i+1}} = 0\right\}_k, \tag{31}$$

$$\left\{\frac{(\psi\rho u)_{j+1/2}^{j+1} - (\psi\rho u)_{j+1/2}^{j}}{\Delta\tau^{j+1}} + \frac{[\rho u(u+Q)]_{i+1}^{j+1} - [\rho u(u+Q)]_i^{j+1}}{h_{i+1}} = -\frac{p_{i+1}^{j+1} + p_i^{j+1}}{h_{i+1}}\right\}_k, \tag{32}$$

$$\begin{aligned}
&\left\{\frac{[\psi\rho(\varepsilon + u^2/2)]_{i+1/2}^{j+1} - [\psi\rho(\varepsilon + u^2/2)]_{i+1/2}^{j}}{\Delta\tau^{j+1}}\right.\\
&\left. + \frac{[\rho(u+Q)(\varepsilon + u^2/2)]_{i+1}^{j+1} - [\rho(u+Q)(\varepsilon + u^2/2)_i^{j+1}]}{h_{i+1}}\right.\\
&\quad \left. = -\frac{(pu)_{i+1}^{j+1} + (pu)_i^{j+1}}{h_{i+1}}\right.
\end{aligned}$$

$$\omega_l = \{q_{l,i},\, q_{l,i+1/2};\ q_{l,i+1} = q_{l,i} + h_{l,i+1},\ q_{l,i+1/2} = q_{l,i} + 0.5h_{l,i+1}$$
$$i = 0, \ldots, N_l - 1,\ q_{l,0} = 0,\ q_{N_l} = q_{sl},\ h_{l,0} = 0, h_{l,N_l+1} = 0\},$$
$$\omega_s = \{q_{s,i},\, q_{s,i+1/2};\ q_{s,i+1} = q_{s,i} + h_{s,i+1},\ q_{s,i+1/2} = q_{s,i} + 0.5h_{s,i+1}$$
$$i = 0, \ldots, N_s - 1,\ q_{s,0} = 0,\ q_{N_s} = q_{sl},\ h_{s,0} = 0, h_{s,N_s+1} = 0\},$$
$$\omega_\tau = \{\tau^j,\ \tau^{j+1} = \tau^j + \Delta\tau^{j+1},\ j = 0, \ldots, J,\ \tau^0 = t_0\}.$$

Box 1.

$$+\frac{1}{h_i}\left(\frac{\lambda_{i+1}^{j+1}}{\psi_{i+1}^{j+1}}\frac{T_{i+3/2}^{j+1} - T_{i+1/2}^{j+1}}{0.5(h_{i+1}+h_i)} - \frac{\lambda_i^{j+1}}{\psi_i^{j+1}}\frac{T_{i+1/2}^{j+1} - T_{i-1/2}^{j+1}}{0.5(h_i+h_{i-1})}\right)\Bigg\}_k, \tag{33}$$

$$\left[\frac{\psi_{i+1/2}^{j+1} - \psi_{i+1/2}^{j}}{\Delta\tau^{j+1}} = -\frac{Q_{i+1}^{j+1} - Q_i^{j+1}}{h_{i+1}}\right]_k, \tag{34}$$

$$\left[\frac{G_{i+1}^{j+1} - G_i^{j+1}}{h_{i+1}} + \alpha(\psi G)_{i+1/2}^{j+1} = 0\right]_k, \tag{35}$$

$$\left[Q_i^{j+1} = -D_i^j\frac{\psi_{i+1/2}^{j+1} - \psi_{i-1/2}^{j+1}}{(h_i + h_{i+1})/2}\right],$$

$$\left[\frac{x_{i+1}^{j+1} - x_i^{j+1}}{h_{i+1}} = \psi_{i+1/2}^{j+1}\right]_k,$$

where $i = 0, \ldots, N_i - 1$ when $k = l$, and $i = 0, \ldots, N_s - 1$ when $k = s$.

The boundary Eqs. (23)–(30) were approximated as follows:

$$q = q_0 : \frac{\psi_{s,0}^{j+1}}{\lambda_{s,0}^{j+1}}\frac{T_{s,0}^{j+1} - T_{s,1/2}^{j+1}}{h_{s,0}/2} = 0,$$

$$u_{s,0} = 0, \qquad Q_{s,0} = 0, \tag{36}$$

$$q = \Gamma_{sl} : (\rho_s v_{sl})^{j+1} = \rho_l^{j+1}(u_s - u_l + v_{sl})^{j+1}, \tag{37}$$

$$(\rho_s v_{sl}^2)^{j+1} + p_s^{j+1} = \rho_l^{j+1}((u_s - u_l + v_{sl})^{j+1})^2 + p_l^{j+1}. \tag{38}$$

$$\frac{\lambda_{s,N-1}}{\psi_{s,N-1}}\frac{T_{s,N-1/2}^{j+1} - T_{s,N-1}^{j+1}}{h_{s,N-1/2}} - \frac{\lambda_{l,0}}{\psi_{l,0}}\frac{T_{l,0}^{j+1} - T_{l,1/2}^{j+1}}{h_{l,1/2}} = L_m(\rho_s v_{sl})^{j+1}, \tag{39}$$

$$T_s = T_l = T_m.$$

$$q = \Gamma_{l\upsilon} : (\rho_\upsilon v_{l\upsilon})^{j+1} = (\rho_\upsilon(u_{l\upsilon} - u_\upsilon + v_{l\upsilon}))^{j+1},$$

$$Q_{l\upsilon}^{j+1} = -(v_{l\upsilon}^{j+1} + u_{l\upsilon}^{j+1}), \tag{40}$$

$$(\rho_{l\upsilon} v_{l\upsilon}^2)^{j+1} + p_{l_\upsilon}^{j+1} = (\rho_\upsilon(u_{l\upsilon} - u_\upsilon + v_{l\upsilon})^2)^{j+1} + p_\upsilon^{j+1}, \tag{41}$$

$$\frac{\lambda_{sur}^{j+1}}{\psi_{sur}^{j+1}}\frac{T_{k,1/2}^{j+1} - T_{sur}^{j+1}}{h_{k,1/2}} = (\rho_{sur} L_\upsilon v_{k_\upsilon})^{j+1} + (\sigma T^4)^{j+1}, \tag{42}$$

$$(G_{l\upsilon})^{j+1} = A(T_{sur}^{j+1})G_0 \exp\left(-4\left(\frac{\tau}{\tau_L}\right)^2\right)^{j+1}. \tag{43}$$

The values at the half-integral nodes for the network functions relating to the integral points are computed as the half-sum of the values at the nearest nodes. Linear interpolation is used for determining the values at nodes with integral subscripts for functions relating to the half-integral points:

$$y_m = \frac{y_{m-1/2}\psi_{m+1/2} + y_{m+1/2}\psi_{m-1/2}}{\psi_{m+1/2} + \psi_{m-1/2}}. \tag{44}$$

THE RESULTS OF THE MODELLING

Let us consider and analyze the changes of the amplitude characteristics of the optoacoustic signals in aluminum and silicon caused by short-pulse laser action.

The shape of the acoustic signal was modelled for a laser pulse of Gaussian shape with width $\tau_L = 3$ ns at half-height, in the range of peak intensities $G_0 = 10^7$–10^{10} W/cm^2. The pressure curves are obtained for a depth of $x_1 = 10$ μm. The point is placed outside the zone of thermal influence of the pulse and on the time interval of interest, and the main signal in it is not distorted by the reflected signal. The chosen range of radiation intensity for the given width τ_L corresponds to the region where the process of melting dominates in both materials, while vaporization has not yet introduced a substantial contribution. A comparative analysis of the optoacoustic signals must give a representation

- of the melting threshold of both materials,
- of the characteristic profile of the optoacoustic signals for metals and semiconductors,
- of how the thermophysical and optical parameters of the irradiated materials affect the dynamics of the phase transitions and the amplitudes of the optoacoustic signals.

There are estimates for the thermal mechanism of sound generation,[1] obtained from a combined solution of the equations of thermal conductivity and hydrodynamics, according to which

$$p(t) = \chi\beta\rho_0\frac{\partial T_{sur}}{\partial t} + \frac{1}{c_p\alpha}\frac{\partial G(t)}{\partial t}, \quad \chi = \frac{\lambda}{c_p\rho_0}. \tag{45}$$

Figures 4(a)–4(c) show the time dependences of the surface temperature, the speed of the melting front, and the pressure for silicon. The modelling showed that, despite the melting temperature, which is higher than in aluminum [T_m^{Si}(1683 K) > T_m^{Al}(933.6 K)], the melting threshold of silicon was lower (Fig. 4(a)). The threshold intensity of laser

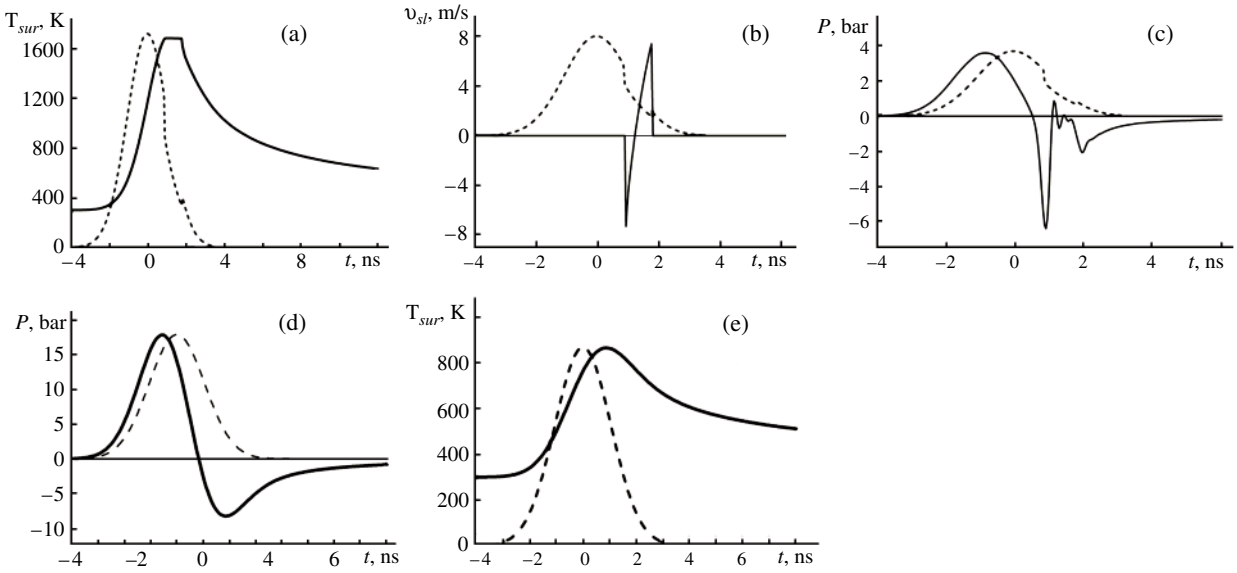

FIG. 4. Time dependence of the surface temperature T_{sur}, the speed of the melting front v_{sl}, and the pressure p for silicon (a, b, c) and aluminum (d, e). The dashed curves denote the time dependence of the absorbed laser energy. The half-width of the laser pulse is 3 ns. For aluminum, $G_0 = 3 \times 10^7$ W/cm^2 and $A = 100\%$; for silicon, $G_0 = 4 \times 10^7$ W/cm^2 and $A = 60\%$.

action was $G_0 = 2.4 \times 10^7$ W/cm^2. Melting temperature on the irradiated silicon surface is reached at the back edge of the laser pulse, Fig. 4(a). Rapid heating of the near-surface layers of silicon promotes a significant decrease of the thermal conductivity in the solid phase as the temperature increases. The appearance of the liquid phase is characterized by the speed v_{sl}, Fig. 4(b), the negative branch of which characterizes melting, while the positive branch characterizes solidification. The optoacoustic signal is a dynamic characteristic that is extremely sensitive to the rate at which energy is introduced into the system. At the initial heating stage, the pressure pulse, Fig. 4(c), is positive. Its magnitude increases with increasing temperature to the value $p_a \approx 3.5$ bar and then slows down because of the decrease of the derivatives $\partial T_{sur}/\partial t$ and $\partial G(t)/\partial t$ and smoothly falls off after changing its sign. The instant at which the liquid phase is formed is characterized by a negative jump of the density $\Delta\rho = \rho_s - \rho_l < 0$, and this shows up on a pressure scan in the form of a sharp dip into the region of negative pressure values, $p_a \approx 7$ bar. The pressure jump associated with the abrupt change of the density at the instant of melting is based on satisfactorily matching this jump with the maximum speed of the melting front, using an elementary estimate of $p = \Delta\rho v_{sl}^2$.[1] Since threshold melting occurs at the back edge of the laser pulse, the melting process, because the radiation intensity rapidly decreases, lasts a short time. The solidification process is accompanied by the evolution of the heat of melting and by a rapid pressure rise, all the way to positive values. After the liquid phase disappears, the optoacoustic signal acquires a slowly varying negative value under the influence of cooling of the target. The melting of the semiconductor in a regime close to the threshold regime is thus characterized by a narrow negative dip in the optoacoustic signal.

Unlike silicon, aluminum, which possess high thermal conductivity, is heated to a great depth, and the temperature on the irradiated surface does not reach the melting temperature, even with a somewhat higher radiation intensity, $G_0 = 3 \times 10^7$ W/cm^2. The shape of the optoacoustic signal in aluminum has the characteristic bipolar shape for metals in the absence of phase transitions, Figs. 4(d) and 4(e). The recorded signal is approximately proportional to the derivative with respect to time of the temperature of the irradiated surface. The positive half-wave corresponds to thermal expansion $\partial T_s/\partial t > 0$, and the negative half-wave to thermal compression $\partial T_s/\partial t < 0$. The amplitude of the positive phase exceeds the amplitude of the negative phase by about a factor of 2 if the laser pulse has a Gaussian shape.[1] The positive half-wave of pressure, characterized by heating, lasts longer in aluminum, and its amplitude is almost a factor of 4 greater than in silicon. The positive half-wave in the optoacoustic signal of aluminum is followed by a negative half-wave, which characterizes the process of cooling the substance. The cooling half-waves of the aluminum and silicon targets approximately coincide in time; however, the signal amplitude is about a factor of 5 greater in aluminum than that in silicon.

The melting threshold for aluminum was recorded at an intensity of $G_0 = 3.5 \times 10^7$ W/cm^2 at the trailing edge of the Gaussian pulse, Figs. 5(a)–5(c). As in silicon, the melting occurs in the negative half-wave of pressure, with the difference that, at the instant the liquid phase is initiated, the density jump in aluminum is positive, $\Delta\rho = \rho_s - \rho_l > 0$. This shows up on the pressure scan in the form of a sharp short jump upwards, all the way to zero pressure p_a. The subsequent solidification occurs with a rapidly varying energy contribution, as a result of which the maximum solidification rate (≈60 m/s) exceeds the maximum melting rate by a factor of 1.5, Fig. 5(b), and exceeds the maximum solidification rate of silicon by a factor of 7.5. Such a high solidification rate sharply increases the negative pressure, $p_a \approx 15$ bar, Fig. 5(c).

When the radiation intensity is increased to $G_0 = 2 \times 10^8$ W/cm^2, the optoacoustic signals of aluminum and silicon change qualitatively: Figs. 6(a)–6(c) and 7(a)–7(c). The time

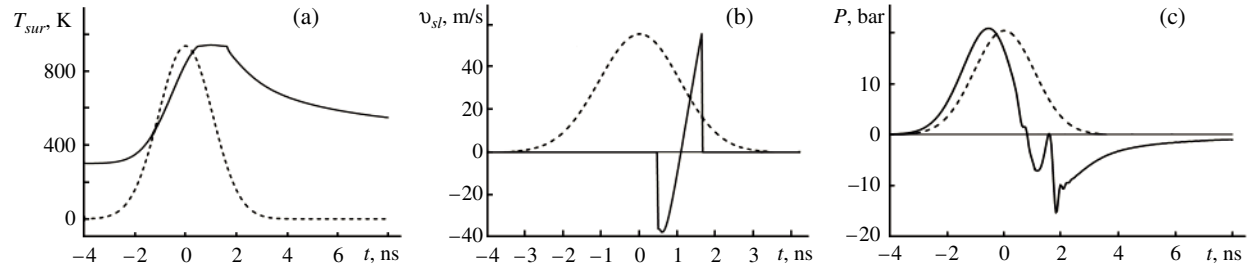

FIG. 5. Time dependence of the surface temperature T_{sur}, the melting rate v_{sl}, and the pressure p for aluminum. The dashed curves denote the time dependence of the absorbed laser-radiation energy. The half-width of the laser pulse is 3 ns. $G_0 = 3.5 \times 10^7$ W/cm^2.

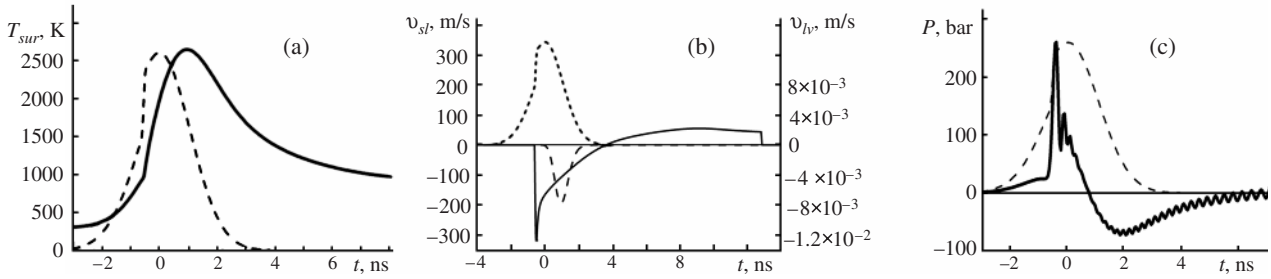

FIG. 6. Time dependence of the surface temperature T_{sur}, the melting rate v_{sl}, the vaporization rate v_{lv}, and the pressure p for aluminum. The dashed curves denote the time dependence of the absorbed energy. The half-width of the laser pulse is 3 ns. $G_0 = 2 \times 10^8$ W/cm^2.

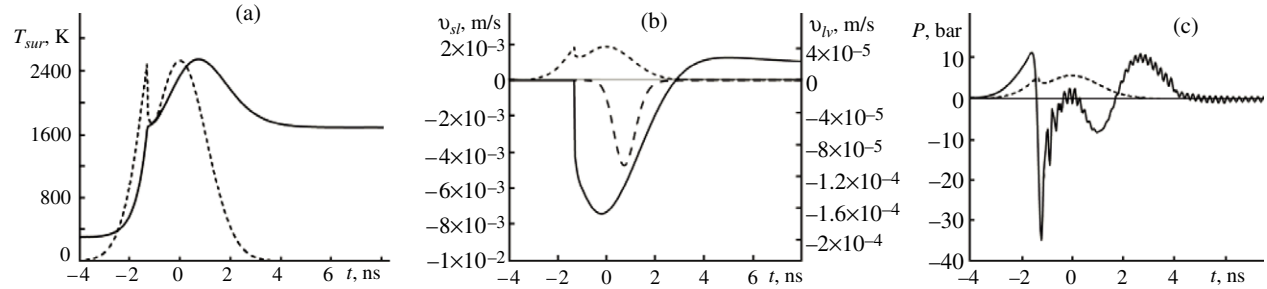

FIG. 7. Time dependence of the surface temperature T_{sur}, the melting rate v_{sl}, the vaporization rate v_{lv}, and the pressure p for silicon. The dashed curves denote the time dependence of the absorbed energy. The half-width of the laser pulse is 3 ns. $G_0 = 2 \times 10^8$ W/cm^2.

of melting is displaced to the leading edge of the laser pulse, where the role of the absorptivity of the material increases. In aluminum, the absorptivity during melting increases abruptly, accelerating the melting rate to 300 m/s, Fig. 6(b); as a consequence, the pressure jumps to 270 bar, Fig. 6(c). The surface in this case is heated to a temperature of $T_{sur}^{\mathrm{Al}} \geq T_b^{\mathrm{Al}}$, and the contribution of the melting becomes appreciable, the rate of which reaches $v_{lv} \approx 8 \times 10^{-3}$ m/s, Fig. 6(b). The amplitude of the optoacoustic pulse quickly falls off after the pressure burst caused by the absorptivity jump and the positive density jump under the combined action of melting, vaporization, and the decrease of the radiation intensity, making a transition to the negative half-wave.

The optoacoustic signal in silicon has an even more complex temporal structure, Figs. 7(a)–7(c). The surface absorptivity for silicon decreases abruptly, Fig. 7(a); in combination with the negative density jump, this increases the negative pressure jump to 35 bar, Fig. 7(c). Continued heating makes it possible to reduce the negative pressure to zero, which then again increases to 10 bar because of the combined action of vaporization, the rate of which ($v_{lv} \approx 4.5 \times 10^{-3}$ m/s, Fig. 7(b)) becomes appreciable, and the reduction of the laser-pulse intensity. The solidification process results in the formation of a positive half-wave with the maximum value of $p_a \approx 10$ bar. Because of the lower absorptivity, the heating rate of the silicon is lower than in aluminum, which is explained by the lower maximum values of the surface temperature, the melting rate, and the pressure jumps.

CONCLUSION

Comparative analysis of the optoacoustic signals caused by laser action on aluminum and silicon, carried out by mathematical modelling, showed that:

1. Melting substantially changes the form of the optoacoustic signal in silicon and aluminum.
2. The pressure jump associated with melting is positive in aluminum ($\Delta p > 0$) and negative in silicon ($\Delta p < 0$).
3. The structure of a time scan of the pressure substantially depends on the action regime. In the case of the threshold

regime, a pressure jump from the melting appears in the negative half-wave of the optoacoustic signal. With radiation intensities that exceed the threshold values, the contribution of melting to the pressure occurs in the form of a narrow dip for silicon or in the form of a narrow burst for aluminum at the stage of heating in the positive half-wave.

4. The threshold intensity of laser radiation that causes melting is lower for silicon than for aluminum, even though the melting temperature of silicon is significantly greater.
5. The optoacoustic signal amplitude is significantly greater for aluminum than for silicon for all the regimes of laser action investigated here.
6. An increase of the laser-pulse intensity from 24 to 200 MW/cm^2 is accompanied by about a 10-fold pressure increase for aluminum and 5-fold for silicon.

ACKNOWLEDGMENTS

This work was carried out with the support of the Russian Foundation for Basic Research (RFFI Projects Nos. 10-07-00246-a and 09-07-0025-a).

[a)]Email: koroleva.on@mail.ru
[b)]Email: specimen@modhef.ru

[1]A. A. Samokhin, "The action of laser radiation on absorbing condensed media," Tr. Inst. Obshch. Fiz. No. 13, 1 (1988).

[2]V. É Gusev and A. A. Karabutov, *Laser Optoacoustics* (Nauka, Moscow, 1991).

[3]S. A. Akhmanov and V. É Gusev, "Laser excitation of supershort acoustic pulses: new possibilities in solid-state spectroscopy, the diagnosis of rapid processes, and nonlinear acoustics," Usp. Fiz. Nauk **162**, No. 3, 3 (1992). [Phys.–Usp. **35**, 153 (1992)].

[4]E. V. Savateeva, A. A. Karabutov, and V. Ya. Panchenko, "Laser optoacoustic spectroscopy of biological tissues," in *Collection of IPLIT, Russian Academy of Sciences. Lasers in Biomedicine* (2005), pp. 183–187.

[5]V. I. Mazhukin, N. M. Nikiforova, and A. A. Samokhin, "Photoacoustic effect accompanying the melting and vaporization of a substance under the action of a laser pulse," Tr. Inst. Obshch. Fiz. **60**, 108 (2004).

[6]V. I. Mazhukin and A. A. Samarskii, "Mathematical modeling in the technology of laser treatments of materials. Review," Surv. Math. Ind. **4**, No. 2, 85 (1994).

[7]D. Crout, "An application of kinetic theory to the problems of evaporation and sublimation of monatomic gases," J. Math. Phys. No. 15, 1 (1936).

[8]V. I. Mazhukin, P. A. Prudkovskiĭ, and A. A. Samokhin, "The gas-dynamic boundary conditions at a vaporization front," Mat. Model. **5**, No. 6, 3 (1993).

[9]V. I. Mazhukin and V. V. Nosov, "Studying how the temperature dependences of the thermophysical and optical characteristics and the equations of state of a metal affect the shape of an optoacoustic signal during laser exposure," Mat. Model. **5**, No. 5, 3 (1993).

[10]V. V. Nosov and V. I. Mazhukin, "How the melting and crystallization processes affect the shape of an optoacoustic signal during laser action on strongly absorbing condensed media," Matematich. Model. **6**, No. 1, 3 (1994).

[11]C. J. Smithells, ed., *Metals Reference Book*, 5th Ed. (Butterworths, London, 1976; Metallurgiya, Moscow, 1980).

[12]I. S. Grigor'eva and E. Z. Meĭlikhova, eds., *Physical Quantities. A Handbook* (Énergoatomizdat, Moscow, 1991).

[13]V. I. Mazhukin, P. V. Breslavskiĭ, and A. V. Shapranov, "Dynamic adaptation in differential equations in partial derivatives of hyperbolic type," in *Encyclopedic Series—Encyclopedia of Low-Temperature Plasma, Ser. B, Reference Applications, Data Bases, and Data Banks, Topical Volume VII-1*, *Mathematical Modelling in a Low-Temperature Plasma, Part 1* (Yanus-K, Moscow, 2008), pp. 190–216.

[14]V. I. Mazhukin and O. N. Koroleva, "Mathematical modelling of laser melting and vaporization of multilayer materials," Zh. Vychislit. Mat. Matematich. Fiz. **46**, 910 (2006).

[15]V. I. Mazhukin and L. Yu. Takoeva, "Principles of the construction of networks in one-dimensional boundary-value problems dynamically adapted to the solution," Mat. Model. **2**, No. 3, 101 (1990).

[16]P. V. Breslavskiĭ and V. I. Mazhukin, "Algorithm for numerically solving the hydrodynamic version of Stefan's problem on adaptive networks," Mat. Model. **3**, No. 10, 104 (1991).

[17]A. N. Tikhonov and A. A. Samarskiĭ, *Equations of Mathematical Physics* (Izd. Mosk. Gos. Univ, Moscow, 1999).